European Radiology (2019) 29:3325–3337
https://doi.org/10.1007/s00330-019-06056-4

IMAGING INFORMATICS AND ARTIFICIAL INTELLIGENCE

A radiomics nomogram may improve the prediction of IDH genotype for astrocytoma before surgery

Yan Tan[1,2] · Shuai-tong Zhang[3,4] · Jing-wei Wei[3,4] · Di Dong[3] · Xiao-chun Wang[1,2] · Guo-qiang Yang[1,2] · Jie Tian[3] · Hui Zhang[1,2]

Received: 1 October 2018 / Revised: 12 December 2018 / Accepted: 31 January 2019 / Published online: 10 April 2019

Abstract

Objectives To develop and validate a radiomics nomogram to preoperative prediction of isocitrate dehydrogenase (IDH) genotype for astrocytomas, which might contribute to the pretreatment decision-making and prognosis evaluating.

Methods One hundred five astrocytomas (Grades II–IV) with contrast-enhanced T1-weighted imaging (CE-T1WI), T2 fluid-attenuated inversion recovery (T2FLAIR), and apparent diffusion coefficient (ADC) map were enrolled in this study (training cohort: $n = 74$; validation cohort: $n = 31$). IDH1/2 genotypes were determined using Sanger sequencing. A total of 3882 radiomics features were extracted. Support vector machine algorithm was used to build the radiomics signature on the training cohort. Incorporating radiomics signature and clinico-radiological risk factors, the radiomics nomogram was developed. Receiver operating characteristic (ROC) curve and area under the curve (AUC) were used to assess these models. Kaplan–Meier survival analysis and log rank test were performed to assess the prognostic value of the radiomics nomogram.

Results The radiomics signature was built by six selected radiomics features and yielded AUC values of 0.901 and 0.888 in the training and validation cohorts. The radiomics nomogram based on the radiomics signature and age performed better than the clinico-radiological model (training cohort, AUC = 0.913 and 0.817; validation cohort, AUC = 0.900 and 0.804). Additionally, the survival analysis showed that prognostic values of the radiomics nomogram and IDH genotype were similar (log rank test, $p < 0.001$; C-index = 0.762 and 0.687; z-score test, $p = 0.062$).

Conclusions The radiomics nomogram might be a useful supporting tool for the preoperative prediction of IDH genotype for astrocytoma, which could aid pretreatment decision-making.

Key Points

- *The radiomics signature based on multiparametric and multiregional MRI images could predict IDH genotype of Grades II–IV astrocytomas.*
- *The radiomics nomogram performed better than the clinico-radiological model, and it might be an easy-to-use supporting tool for IDH genotype prediction.*
- *The prognostic value of the radiomics nomogram was similar with that of the IDH genotype, which might contribute to prognosis evaluating.*

Keywords Astrocytoma · Radiomics · Nomogram · Isocitrate dehydrogenase · Survival

Yan Tan and Shuai-tong Zhang contributed equally to this work.

Electronic supplementary material The online version of this article (https://doi.org/10.1007/s00330-019-06056-4) contains supplementary material, which is available to authorized users.

✉ Jie Tian
tian@ieee.org

✉ Hui Zhang
zhanghui_mr@163.com

[1] Department of Radiology, The first hospital of Shanxi Medical University, Taiyuan 030001, Shanxi Province, China

[2] Department of Medical Imaging, Shanxi Medical University, Taiyuan 030001, Shanxi Province, China

[3] Key Laboratory of Molecular Imaging, Chinese Academy of Sciences, Institute of Automation, Beijing 100190, China

[4] University of Chinese Academy of Sciences, Beijing 100080, China

Abbreviations

ADC	Apparent diffusion coefficient
AUC	Area under the curve
CE-T1WI	Contrast-enhanced T1-weighted images
IDH	Isocitrate dehydrogenase
IDH-M	Isocitrate dehydrogenase mutant type
IDH-W	Isocitrate dehydrogenase wild type
LASSO	Least absolute shrinkage and selection operator
LOOCV	Leave-one-out cross-validation
OS	Overall survival
RFE	Recursive feature elimination
ROC	Receiver operating characteristic
ROI	Regions of interest
SVM	Linear support vector machine
T2FLAIR	T2 fluid-attenuated inversion recovery images

Introduction

Astrocytomas are the most common type of diffuse glioma and are associated with poor prognosis [1]. The 2016 World Health Organization (WHO) Classification of Tumors of the Central Nervous System (CNS) classifies astrocytomas into isocitrate dehydrogenase (IDH)-wild type (IDH-W) and IDH-mutant type (IDH-M), while the genotype for oligodendroglioma or oligoastrocytoma is defined both by IDH and 1p/19q [2, 3]. IDH genotype is an important genetic hallmark with considerable prognostic value for astrocytomas [2–4]. Besides IDH-M astrocytomas are more amenable to gross-total resection [5] and have better responses to standard chemo- or radio-therapy [6, 7], they also have extra opportunity for targeted therapy via inhibitors of the IDH-M enzyme [8]. Recently, targeted therapeutic strategies for IDH-M astrocytomas have entered phase I clinical trials [9]. Thus, early determination of IDH genotype can facilitate this pretreatment decision-making. Currently, the IDH genotype is mainly identified by sequencing or immunohistochemistry with tumor samples, which can be only obtained postoperatively. Even the biopsy for unresectable astrocytomas also runs the risk of neurological deficits and the obtained small sample cannot reflect the whole heterogeneity of the entire tumor. Thus, to overcome these limitations, the creation of a noninvasive technology to identify the IDH genotype of the tumor is urgently needed.

Neuroimaging may be an alternative for noninvasive determination of IDH genotype especially for the unresectable astrocytomas [10–12], which has been attempted [13, 14], but it remains a challenge. Conventional MRI characteristics, including unilateral growth, sharpness of tumor margin, and heterogeneous intensity, are highly related to IDH genotype and prognosis [13, 14]. However, these analyses lack satisfactory accuracy and are dependent on radiologists' subjective judgment. Radiomics has the combined advantages of being highly patient-specific and noninvasive, it could mine high-throughput quantitative features from conventional medical images that applied in clinical decision support systems to improve diagnostic, prognostic, and predictive accuracy [15, 16]. Recent studies have reported that radiomics is a useful approach to estimate IDH genotype for Grade II gliomas [17–19] or high-grade gliomas [20, 21]. These studies need postoperative diagnosis of tumor grading as a prerequisite for estimating IDH status, which would limit the preoperative application in clinical. Furthermore, Baldock et al [22] reported that the tumor growth models based on MRI semantic characteristics could identify the IDH genotype of Grades II–IV gliomas. To date, the prediction of IDH genotype for a combined cohort of Grades II–IV astrocytomas by radiomics has not been attempted. We hypothesized that the radiomics approach could also predict the IDH genotype of Grades II–IV astrocytomas and contains the prognostic information.

Accordingly, the aim of the present study was to develop and validate a radiomics nomogram for preoperative prediction of IDH genotype in astrocytomas and analyze its corresponding prognostic value in overall survival (OS).

Materials and methods

Patients

The institutional review board of our institution approved this study protocol. Given the retrospective study and anonymous patient data, informed consents were waived. According to the inclusion and exclusion criteria (Supplementary S1), 105 patients with surgery were obtained between October 2011 and March 2017. The recruitment pathway for patients in this study is presented in Supplementary S1. All these cases were split into the training cohort ($n = 74$) and the validation cohort ($n = 31$) by stratified sampling using computer-generated random numbers at a ratio of 7:3. IDH1/2 mutations were determined using Sanger sequencing, and the details are shown in Supplementary S2.

To assess the prognostic value of the predictive model for IDH genotype, OS was calculated as the time from the initial diagnosis until death or censure point (August 18, 2018) if patients were still alive. The minimum follow-up period to ascertain the OS for alive patients was the median survival of each tumor grade (605 days for Grade II, 398 days for Grade III, and 169 days for Grade IV) after the initial diagnosis. Finally, 61 of 105 patients were included. The clinical characteristics of these 61 patients including age, gender, grade, treatment, IDH genotype, and OS were collected and compared between risk groups stratified by the model. The flowchart of this study is shown in Fig. 1.

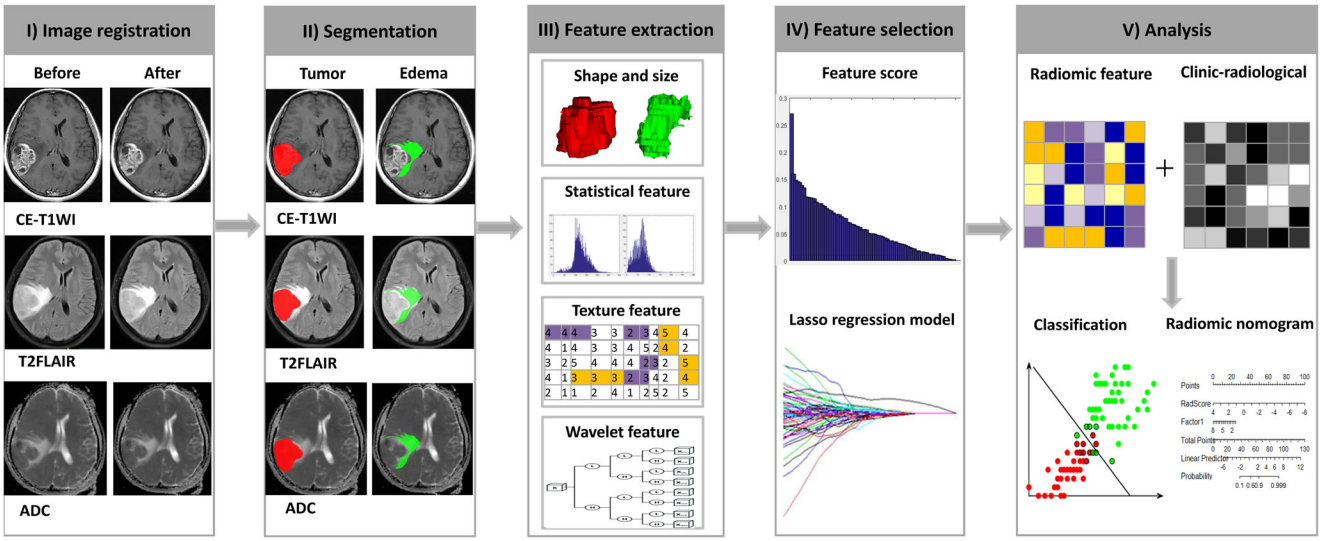

Fig. 1 A flowchart describing the radiomics method for IDH genotype prediction. (I) T2FLAIR and ADC images were co-registered to the corresponding CE-T1WI images by using FSL-FLIRT. (II) Regions of interests (ROI) of the tumor lesion and peritumoral edema area were manually delineated. (III) Radiomics features were extracted including shape and size features, first-order statistics features, textural features, and textural and wavelet features after local standard deviation filter. (IV) Discriminative features were selected by the LASSO regression model. (V) Prediction model was constructed by incorporating both radiomics signature and clinico-radiological characteristics; ROC curves and boxplot maps were performed for further statistical analyses; a nomogram was finally adopted to present the outcomes of IDH prediction with a clinical usefulness

MRI data acquisition

Preoperative MRI was performed with a 3.0 T scanner (GE Signa HDxt) using an 8-channel array coil. Contrast-enhanced T1-weighted imaging (CE-T1WI), T2 fluid-attenuated inversion recovery (T2FLAIR), and apparent diffusion coefficient (ADC) sequences were used for the following analysis. The parameters were repetition time (TR) 195 ms and echo time (TE) 4.76 ms for gradient-echo (GRE) CE-T1WI; TR 8000 ms, TE 95 ms, and inversion time (TI) 2000 ms for T2FLAIR. Slice thickness and slice interval were 5.0/1.5 mm. Field of view (FOV) was 240 × 240 mm^2; matrix, 256 × 256. About 0.1 mmol/kg of gadolinium chelate contrast was injected for contrast-enhanced imaging. Parameters for DWI data: echo planar imaging (EPI) sequence was used to perform DWI. Implemented *b* values were 0 and 1000 mm^2/s. TR/TE, 3000/87 ms; FOV, 240 × 240 mm^2; matrix, 160 × 160; slice thickness, 6 mm; slice interval, 1 mm; NEX = 2. The original DWI maps were transmitted to ADW4.4 (Advanced Workstation 4.4) to generate axial ADC maps using GE software processing.

Image co-registration and ROI segmentation

The T2FLAIR and ADC images were co-registered to the corresponding CE-T1WI images using affine transformation through the Oxford center for Functional MRI of the Brain (FMRIB) Linear Image Registration Tool (FLIRT) of FMRIB Software Library (FSL) [23]. Manual segmentation was fulfilled slice by slice on axial MRI images to obtain volumetric datasets using ITK-SNAP (http://www.itksnap.org); the ROIs of tumor area were delineated on CE-T1WI images, and the ROIs of peritumoral edema were delineated on T2FLAIR images by a neuroradiologist (XCW) with 15 years of experience, and confirmed by another neuroradiologist with 30-year experience (HZ), then transferred to corresponding other two MRI images. The detailed ROIs segmentation of the MRI images is showed in Supplementary S3.

As the results of radiomics feature calculation depend on the contours of ROIs delineated by radiologists, both test-retest analysis and inter-radiologist analysis should be applied to evaluate the robustness of all the features. Based on randomly chosen 30 patients, the test-retest analysis was performed where ROIs for each patient were segmented twice by one radiologist with 15 years of experience. The dataset used for interrater analysis included the above chosen 30 patients, where ROIs for each patient were segmented by two radiologists with 15 and 30 years of experience independently. The radiomics features extracted from these ROIs were assessed using the intraclass correlation coefficient (ICC).

Radiomics feature extraction

A total of 647 radiomics features, consisting of 8 shape and size features, 17 first-order statistics features, 54 textural features for the original image set, and first-order statistics and textural features for 8 wavelet filtered image sets were extracted [24–31]. We extracted this radiomics feature set from the tumor lesion and peritumoral edema area on CE-T1WI, T2FLAIR, and ADC maps, respectively. Thus, a total of

3882 features were obtained. A detailed description of the calculated radiomics features is provided in Supplementary S4. Features with ICCs both test-retest and inter-raters reproducibility analysis larger than 0.75 were remained for the following analysis.

Radiomics feature selection

To reduce irrelevant and redundant information, a three-stage feature selection was performed in the training cohort. First, a Mann–Whitney *U* test was performed and features with $p < 0.1$ were selected as potential predictive ones. The least absolute shrinkage and selection operator (LASSO) feature selection algorithm was then conducted to select the most useful predictive features in the training cohort for CE-T1WI, T2FLAIR, and ADC, respectively. Chalkidou et al [32] proposed that at least 10 to 15 observations per predictor variable were required to build a reasonably stable model. Thus, recursive feature elimination (RFE) feature selection was performed to avoid further over-fitting.

Development of radiomics models

The linear support vector machine (SVM) was adopted to predict the IDH genotype based on the selected MRI features in the training cohort for CE-T1WI, T2FLAIR, and ADC, respectively. Fivefold cross-validation was performed to determine the optimal regulation parameter C, which controlled the trade-off between the accuracy in the training cohort and model complexity. With the optimal C, the radiomics models based on selected CE-T1WI, T2FLAIR, and ADC features were fitted to the training cohort and further validated in the validation cohort. Finally, a CE-T1WI + T2FLAIR + ADC model was built based on the features in CE-T1WI, T2FLAIR, and ADC models using RFE with SVM. The output of the best radiomics model was regarded as the radiomics signature. Stratified analysis was conducted to show whether the radiomics signature had similar predictive value in low- or high-grade astrocytomas, respectively.

Development of clinico-radiological model

The clinical characteristics of gender, grade, and age were studied. The semantic radiological characteristics were assessed by the radiologist with 15 (XCW) years of experience, which included tumor size (largest diameter), border (well or ill defined), hemorrhage (yes or no), cystic and necrosis (no, ≤ 25%, 25–50%, ≥ 50%), edema degree (largest diameter), enhancement style (no, ring, nodular, irregular) and degree (no, slight, obvious), signal characteristics (homogeneous, heterogeneous), tumor location (left or right hemisphere, frontal, occipital, parietal, temporal, insular, or multilobe), cross midline growth (yes or no), involving deep white matter (yes or no), involving pia mater (yes or no), involving ependymal membrane (yes or no). Univariate analysis was conducted to determine potential clinico-radiological characteristics which were significantly different between IDH-M and IDH-W groups in the training and validation cohorts. Multivariate logistic regression with forward selection was performed on the training cohort to build the clinico-radiological model.

Development of the radiomics nomogram

Incorporating the radiomics signature and characteristics in the clinico-radiological model, the combined model was built using the logistic regression method with forward stepwise selection. To provide the clinician and patients with an individualized and easy-to-use tool for preoperative prediction of the IDH genotype, the combined model was visualized as the radiomics nomogram.

Assessment of predictive models

The performances of these predictive models were first assessed on the training cohort and then validated on the validation cohort using receiver operating characteristic (ROC) curve. Calibration curve and Hosmer–Lemeshow test were used to assess the agreement between nomogram prediction probabilities of the IDH genotype and actual outcomes. To assess the difference between the radiomics nomogram and the clinico-radiological model, the DeLong test was performed.

Survival analysis

To assess the prognostic value of the radiomics nomogram, Kaplan–Meier survival analysis and log rank test were performed. C-index of the radiomics nomogram was also calculated. To compare the difference in prognostic values between the radiomics nomogram and IDH genotype, a *z*-score test was applied.

Statistical analysis

Statistical analysis was performed using a PASW Statistics version 18.0 (SPSS Inc.) for Windows (Microsoft Corporation) and R version 3.4.1. For continuous clinico-radiological factors, the Levene test was used to assess the equality of variances between the IDH-M and IDH-W groups, and Student's *t* test or Welch's *t* test was used to test between-group differences. For categorical factors, Pearson's chi-square test was used. $P < 0.05$ was statistically significant. The packages in R software involved in this study are shown in Supplementary S5.

Results

Patients' demographic data, clinico-radiological characteristics

Patients' demographic data, clinico-radiological characteristics of astrocytomas in training and validation cohorts are shown in Supplementary S6. We included 51 (48.57%) cases of IDH-M patients and 54 (51.43%) cases of IDH-W patients. There was no significant difference for the IDH status distribution in the training and validation cohorts ($p = 0.850$).

There were no significant differences ($p = 0.149$–0.976) in all clinico-radiological characteristics between the training and validation cohorts, which justified their use as study cohorts.

Radiomics feature robustness and selection

After analysis of reproducibility to avoid effect of intra/interrater variation, 632 radiomic features on tumor region and 429 features on edema region were remained for CE-T1WI images; 618 tumor features and 314 edema features for T2FLAIR images; and 624 tumor features and 266 edema features for ADC map. There were 496 tumor features and 223 edema features with $p < 0.1$ for CE-T1WI images, 254 tumor features and 165 edema features for T2FLAIR images, and 241 tumor features and 149 edema features for ADC images (Fig. S3, Supplementary S7). In the second stage of feature selection, the 5, 12, and 11 radiomics features were selected using LASSO for CE-T1WI, T2FLAIR, and ADC images, respectively (Supplementary S8). To avoid further over-fitting, RFE with SVM was performed for T2FLAIR and ADC images, and three radiomics features were selected for T2FLAIR and ADC images, respectively. For CE-T1WI + T2FLAIR + ADC images, six features were selected. The selected radiomics features for CE-T1WI, T2FLAIR, ADC, and CE-T1WI + T2FLAIR + ADC images are listed in Table 1.

Performance of the radiomics models

The CE-T1WI, T2FLAIR, ADC, and CE-T1WI + T2FLAIR + ADC models yielded the AUC values of 0.896, 0.789, 0.777, and 0.901 in the training cohort, and 0.867, 0.771, 0.800, and 0.888 in the validation cohort, respectively. ROC curves and boxplots are shown in Fig. 2. The accuracy, sensitivity, and specificity of radiomics models are shown in Table 2. Due to the best performance, the CE-T1WI + T2FLAIR + ADC model was selected as the final radiomics model, and the formula of the radiomics signature of the final radiomics model is shown in Supplementary S9.

Table 1 The results of radiomics feature selection based on cross-validation

MRI sequences	Feature number	Individual features
CE-T1WI	5	T1_Edema_Coif2_glrlm_RP ($p = 0.007$)
		T1_Edema_Coif1_glszm_GLN ($p < 0.001$)
		T1_Tumor_Coif1_glrlm_SRLGLE ($p < 0.001$)
		T1_Tumor_Coif2_fos_median ($p = 0.007$)
		T1_Tumor_Coif2_ngtdm_strength ($p = 0.038$)
T2FLAIR	3	T2_Edema_Coif8_glszm_SAE ($p = 0.002$)
		T2_Tumor_Coif8_glszm_SAE ($p < 0.001$)
		T2_Tumor_Coif4_glszm_GLV ($p = 0.049$)
ADC	3	ADC_Edema_Ori_glszm_SZN ($p = 0.009$)
		ADC_Tumor_Coif1_glszm_SAE ($p = 0.005$)
		ADC_Tumor_Coif4_glszm_GLV ($p = 0.025$)
CE-T1WI + T2FLAIR + ADC	6	T1_Edema_Coif2_glrlm_RP ($p = 0.007$)
		T1_Tumor_Coif2_fos_median ($p = 0.007$)
		T1_Edema_Coif1_glszm_GLN ($p < 0.001$)
		T2_Tumor_Coif8_glszm_SAE ($p = 0.001$)
		ADC_Tumor_Coif1_glszm_SAE ($p = 0.005$)
		ADC_Tumor_Coif4_glszm_GLV ($p = 0.025$)

P value for each radiomic feature associated with IDH mutation status was calculated using Mann–Whitney *U* test

CE-T1WI contrast-enhanced T1-weighted image, *T2FLAIR* T2 fluid-attenuated inversion recovery image, *ADC* apparent diffusion coefficient, *glrlm* gray-level run-length matrix, *glszm* gray-level size-zone matrix, *fos* first order of statistic, *ngtdm* neigboring gray tone difference matrix, *RP* run percentage, *GLN* gray-level nonuniformity, *SRLGLE* short run low gray-level emphasis, *SAE* small area emphasis, *SZN* size-zone nonuniformity, *GLV* gray-level variance

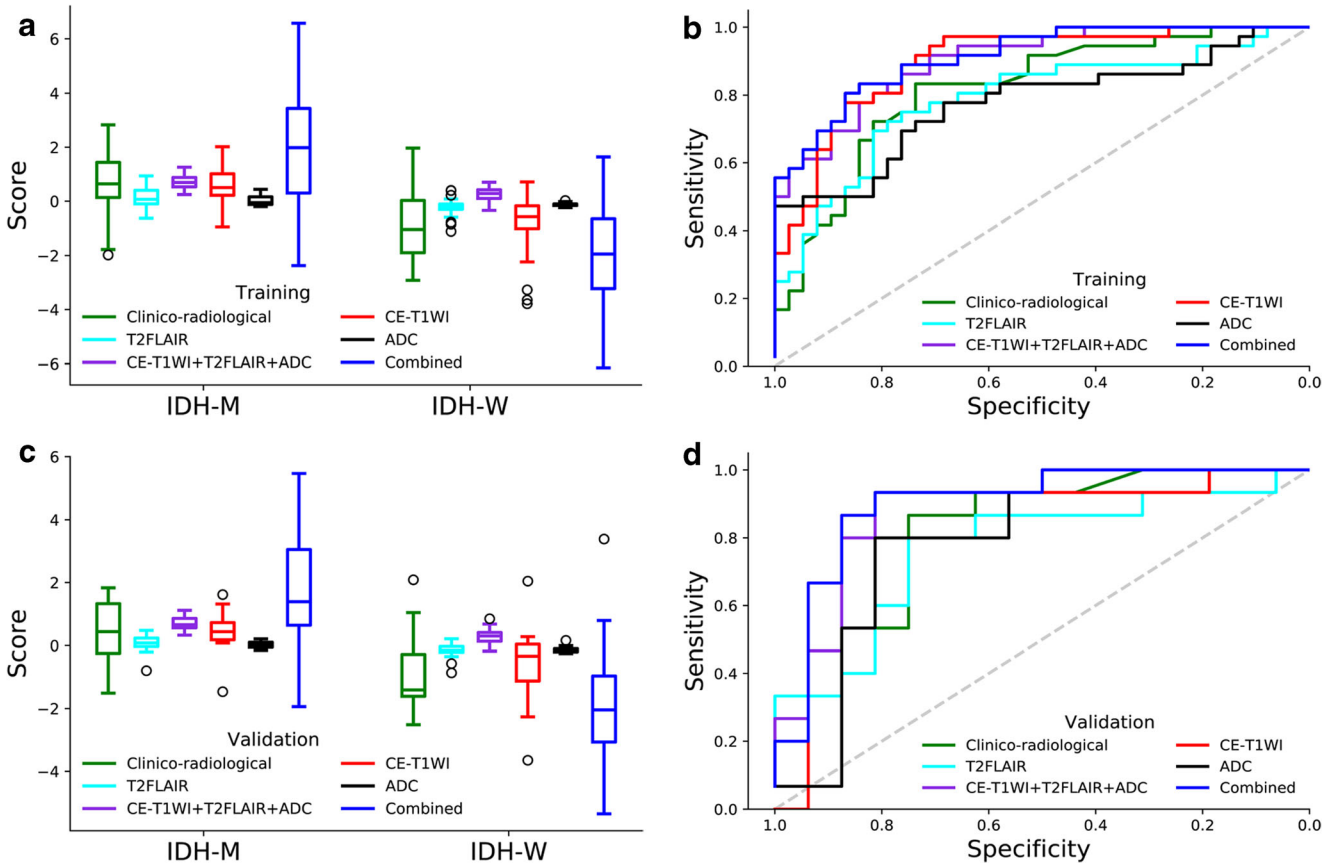

Fig. 2 The boxplots (**a**) and ROC curves (**b**) of the clinico-radiological model, radiomics models of CE-T1WI, T2FLAIR, ADC, and T2FLAIR + ADC + CE-T1WI, and combined model in the training cohort. The boxplots (**c**) and ROC curves (**d**) of the clinico-radiological model, radiomics models of CE-T1WI, T2FLAIR, and ADC, T2FLAIR + ADC + CE-T1WI, and combined model in the validation cohort

Table 2 The performance of the clinico-radiological model, radiomics models, and combined model

Model	Performance	AUC	SEN	SPE	ACC	*p* value	Cutoff
Clinico-radiological	Training cohort	0.817 (0.794–0.839)	0.833	0.737	0.784	7E−7	− 0.099
	Validation cohort	0.804 (0.747–0.862)	0.667	0.750	0.710	0.002	− 0.099
CE-T1WI	Training cohort	0.896 (0.880–0.913)	0.972	0.684	0.824	8E−9	− 0.256
	Validation cohort	0.867 (0.813–0.920)	*0.933*	0.625	0.774	8E−4	− 0.256
T2FLAIR	Training cohort	0.789 (0.764–0.813)	0.750	0.763	0.757	2E−5	− 0.092
	Validation cohort	0.771 (0.710–0.832)	0.867	0.563	0.710	0.047	− 0.092
ADC	Training cohort	0.777 (0.752–0.802)	0.472	1.000	0.743	2E−5	0.023
	Validation cohort	0.800 (0.741–0.859)	0.467	*0.875*	0.677	0.005	0.023
CE-T1WI + T2FLAIR + ADC	Training cohort	0.901 (0.886–0.916)	0.917	0.711	0.811	8E−11	0.405
	Validation cohort	0.888 (0.845–0.930)	*0.933*	0.813	0.806	9E−5	0.405
Combined	Training cohort	*0.913 (0.899–0.927)*	0.833	0.842	0.838	8E−12	− 0.056
	Validation cohort	0.900 (0.859–0.941)	0.867	*0.875*	*0.871*	*2E−5*	− 0.056

AUC area under the curve, *SEN* sensitivity, *SPE* specificity, *ACC* accuracy, *CE-T1WI* contrast-enhanced T1-weighted image, *T2FLAIR* T2 fluid-attenuated inversion recovery image, *ADC* apparent diffusion coefficient

The best performance in validation cohort is indicated in italics; the CE-T1WI + T2FLAIR + ADC model was built based on the imaging features selected from those in T1WI, T2FLAIR, or ADC model using forward stepwise selection; the combined model was built based on the imaging features in CE-T1WI + T2FLAIR + ADC model and the clinic-radiological risk factors using logistic regression. The cutoff values were determined based on the output value of each predictive model in the training cohort

In addition, the stratified analysis showed that the CE-T1WI + T2FLAIR + ADC model performed well in IDH prediction for low-grade (Grade II) or high-grade (Grades III–IV) astrocytoma (training cohort, AUC = 0.874 and 0.928; validation cohort, AUC = 1.000 and 0.722; [Fig. 3]).

Performance of the clinico-radiological model

Significant differences existed in age ($p < 0.001$), grade ($p = 0.038$), edema degree ($p = 0.004$), enhancement style ($p < 0.001$), and enhancement degree ($p = 0.006$) between the IDH-M and IDH-W groups in the training cohort by univariate analysis (Table 3). However, age ($p = 0.002$), enhancement style ($p = 0.031$), and enhancement degree ($p = 0.001$) were selected by multivariate analysis to develop the clinico-radiological model. The radiological characteristics of IDH-W and IDH-M astrocytomas are shown in Fig. 4.

The clinico-radiological model for IDH prediction yielded AUC values of 0.817 and 0.804 in the training and validation cohorts, respectively. The sensitivity, specificity, and accuracy of the clinico-radiological model were summarized in Table 2**.** ROC curves and boxplots are shown in Fig. 2.

Performance of the radiomics nomogram

During the development of combined model, radiomics signature and age were selected. Compared with the radiomics models and clinico-radiological model, the combined model reached the highest AUC (training cohort, 0.913 [95% CI 0.889–0.920]; validation cohort, 0.900 [95% CI 0.838–0.920], Table 2 and Fig. 2). The DeLong tests revealed a significant difference between the clinico-radiological model and combined model in the training and validation cohorts ($p = 0.004$ and 0.036).

The radiomics nomogram for visualization of the combined model is shown in Fig. 5. The calibration curves of the radiomics nomogram demonstrated satisfactory agreement between the predictive and observational possibility of the IDH genotype in both the training and validation cohorts ($p = 0.737$ and 0.401; Hosmer–Lemeshow test).

Survival analysis

The clinical characteristics of these 61 patients are shown in Table 4, where high-risk (< 0.056 cutoff) and low-risk (≥ 0.056 cutoff) groups are defined based on the cutoff score (0.056) of the combined model. KM analysis showed that both IDH genotype and combined model provided statistically significant discrimination between the high- and low-risk groups ($p < 0.001$ [log rank test]) (Fig. 6). In addition, IDH genotype and combined model yielded C-index values of 0.687 and 0.762, and the z-score test showed that the prognostic value had no statistical difference between the IDH genotype and combined model ($p = 0.062$).

Discussion

In our study, the radiomics signature based on multiparametric and multiregional MRI images could predict IDH genotype for Grades II–IV astrocytomas. The radiomics nomogram incorporating the radiomics signature and age performed better than the clinico-radiological model, which demonstrated the incremental value of the radiomics signature in predicting IDH genotype for astrocytomas. Furthermore, the combined model stratified astrocytomas into high-risk and low-risk groups according to OS, and its prognostic performance was similar to that of IDH genotype.

The combined six radiomics features extracted from the multiparametric and multiregional MR images could accurately predict the IDH genotype, and performed better than a single sequence or region. CE-T1WI contains information of regional angiogenesis and the destruction of the blood-brain barrier in the tumor. T2FLAIR reflects the anatomical information of tumor, and ADC provides the information about architecture and density of tumor cells. The combined radiomics features from these sequences could quantify the comprehensive information to characterize the heterogeneity of the glioma. Furthermore, the radiomics features are both from the tumor and edema area contributing to predict the IDH genotype in our study, while other radiomics studies of

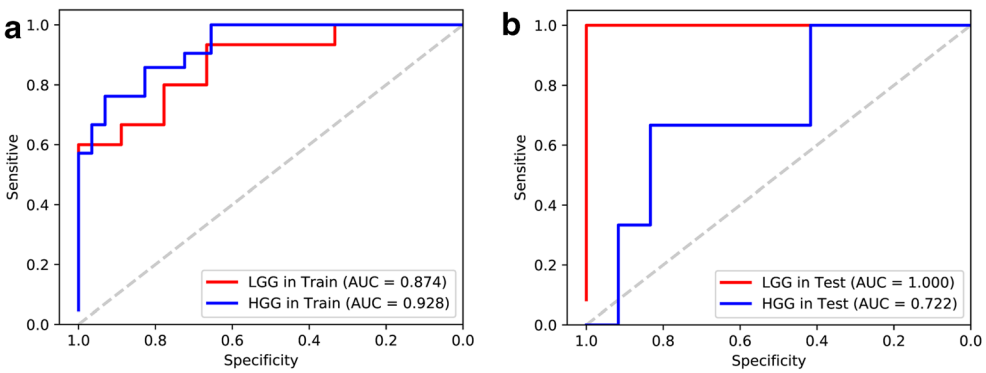

Fig. 3 Stratified analyses in low-grade astrocytoma and high-grade astrocytoma by the CE-T1WI + T2FLAIR + ADC model in training cohort (**a**) and test cohort (**b**)

Table 3 Patients' clinical and radiological characteristics by univariate analyses

Characteristics	Training cohort ($N = 74$)		p value	Validation cohort ($N = 31$)		p value
	IDH-M	IDH-W		IDH-M	IDH-W	
IDH genotype	36 (48.65%)	38 (51.35%)		15 (48.39%)	16 (51.61%)	
Gender			0.852†			0.206†
Male	21 (58.33%)	24 (63.16%)		5 (33.33%)	10 (62.50%)	
Female	15 (41.67%)	14 (36.84%)		10 (66.67%)	6 (37.50%)	
Grade			0.252†			0.009†
II	15 (41.67%)	9 (23.68%)		12 (80.00%)	4 (25.00%)	
III	14 (38.89%)	20 (52.63%)		2 (13.33%)	8 (50.00%)	
IV	7 (19.44%)	9 (23.68%)		1 (6.67%)	4 (25.00%)	
Age (years)	42.36 ± 10.90	53.21 ± 13.19	< 0.001*	45.73 ± 11.28	54.31 ± 11.58	0.053*
Tumor size (cm)	6.28 ± 1.87	6.02 ± 1.66	0.534*	6.50 ± 2.26	5.68 ± 1.33	0.240*
Border			0.520†			0.499†
Well-defined	8 (22.22%)	12 (31.58%)		3 (20.00%)	6 (37.50%)	
Ill-defined	28 (77.78%)	26 (68.42%)		12 (80.00%)	10 (62.50%)	
Hemorrhage			0.077†			0.953†
Yes	5 (13.89%)	13 (34.21%)		1 (6.67%)	2 (12.50%)	
No	31 (86.11%)	25 (65.79%)		14 (93.33%)	14 (87.50%)	
Cystic and necrosis			0.853†			0.745†
No	12 (33.33%)	11 (28.95%)		5 (33.33%)	4 (25.00%)	
≤ 25%	9 (25.00%)	13 (34.21%)		4 (26.67%)	7 (43.75%)	
25%–50%	8 (22.22%)	7 (18.42%)		2 (13.33%)	1 (6.25%)	
≥ 50%	7 (19.44%)	7 (18.42%)		4 (26.67%)	4 (25.00%)	
Edema degree	1.09 ± 1.55	2.15 ± 1.45	0.004*	1.04 ± 1.35	2.67 ± 1.28	0.002*
Enhancement style			< 0.001†			0.018†
No	14 (38.89%)	3 (7.89%)		4 (26.67%)	1 (6.25%)	
Ring enhancement	10 (27.78%)	27 (71.05%)		3 (20.00%)	11 (68.75%)	
Nodular enhancement	6 (16.67%)	6 (15.79%)		6 (40.00%)	1 (6.25%)	
Irregular enhancement	6 (16.67%)	2 (5.26%)		2 (13.33%)	3 (18.75%)	
Enhancement degree			0.0006†			0.072†
No	14 (38.89%)	3 (7.89%)		4 (26.67%)	1 (6.25%)	
Slight	3 (8.33%)	3 (7.89%)		2 (13.33%)	0 (0.00%)	
Obvious	19 (52.78%)	32 (84.21%)		9 (60.00%)	15 (93.75%)	
Signal characteristics			0.721†			0.953†
Homogeneous	3 (8.33%)	3 (7.89%)		2 (13.33%)	1 (6.25%)	
Heterogeneous	33 (91.67%)	35 (92.11%)		13 (86.67%)	15 (92.75%)	
Tumor location (1)			0.826†			0.862†
Left hemisphere	17 (47.22%)	18 (47.37%)		8 (53.33%)	8 (50.00%)	
Right hemisphere	19 (52.78%)	20 (52.63%)		7 (46.67%)	8 (50.00%)	
Tumor location (2)			0.064†			0.694†
Frontal lobe	19 (52.78%)	11 (28.95%)		7 (46.67%)	6 (37.50%)	
Occipital lobe	0 (0.00%)	1 (2.63%)		0 (0.00%)	2 (12.50%)	
Parietal lobe	5 (13.89%)	4 (10.53%)		2 (13.33%)	2 (12.50%)	
Temporal lobe	1 (2.78%)	7 (18.42%)		1 (6.67%)	2 (12.50%)	
Insular lobe	0 (0.00%)	0 (%)		0 (0.00%)	1 (6.25%)	
Multilobe	11 (30.56%)	15 (39.47%)		5 (33.33%)	3 (18.75%)	
Cross midline growth			0.614†			0.714†
Yes	5 (13.89%)	8 (21.05%)		3 (20.00%)	3 (18.75%)	
No	31 (86.11%)	30 (78.95%)		12 (80.00%)	13 (81.25%)	

Table 3 (continued)

Characteristics	Training cohort ($N = 74$)		p value	Validation cohort ($N = 31$)		p value
	IDH-M	IDH-W		IDH-M	IDH-W	
Involving deep white matter			0.266†			0.937†
Yes	29 (80.56%)	35 (92.11%)		12 (80.00%)	14 (87.50%)	
No	7 (19.44%)	3 (7.89%)		3 (20.00%)	2 (12.50%)	
Involving pia mater			0.578†			0.953†
Yes	32 (88.89%)	31 (81.58%)		14 (93.33%)	14 (87.50%)	
No	4 (11.11%)	7 (18.42%)		1 (6.67%)	2 (12.50%)	
Involving ependymal membrane			0.134†			0.609†
Yes	10 (27.78%)	18 (47.37%)		7 (46.67%)	5 (31.25%)	
No	26 (72.22%)	20 (52.63%)		8 (53.33%)	11 (68.75%)	

P value < 0.05 was considered as a significant difference

* represented Student's t test. † represented the Pearson's test

IDH prediction only focused on the tumor area [17–19, 21]. Recent studies showed that radiomics features from peritumoral regions could capture the heterogeneity to predict prognosis for glioblastoma [33, 34], which might also be related to the IDH genotype. It confirms that IDH mutations can convert α-ketoglutarate to 2-hydroxyglutarate [35, 36], which ultimately suppresses angiogenesis and cell proliferation [37]. This suggests that IDH-W astrocytomas have more aggressive behavior than that of IDH-M tumors, which results in less invasive tumor cells in the edema area of IDH-M astrocytomas. The current combined six radiomics features could more accurately reflect this whole information of angiogenesis and cell proliferation both in tumor and edema regions than a single sequence or region. We also found that the radiomics

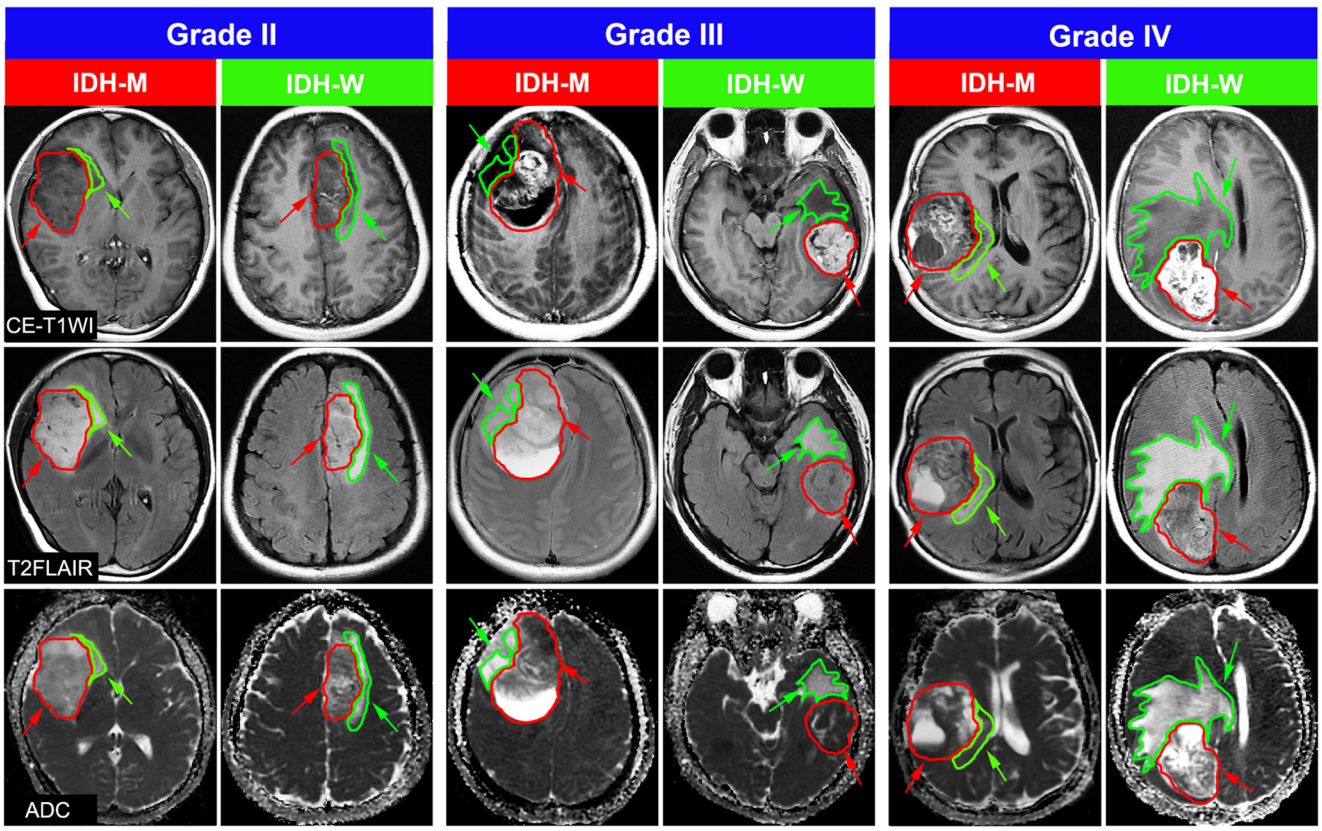

Fig. 4 The radiological characteristics of IDH-W and IDH-M astrocytomas. The edema area was larger and enhancement degree was obvious in the IDH-W group than the IDH-M group for Grades II, III, and IV astrocytoma, respectively. The green curves and arrows represent the area of edema, and the red curves and arrows represent the area of the tumor

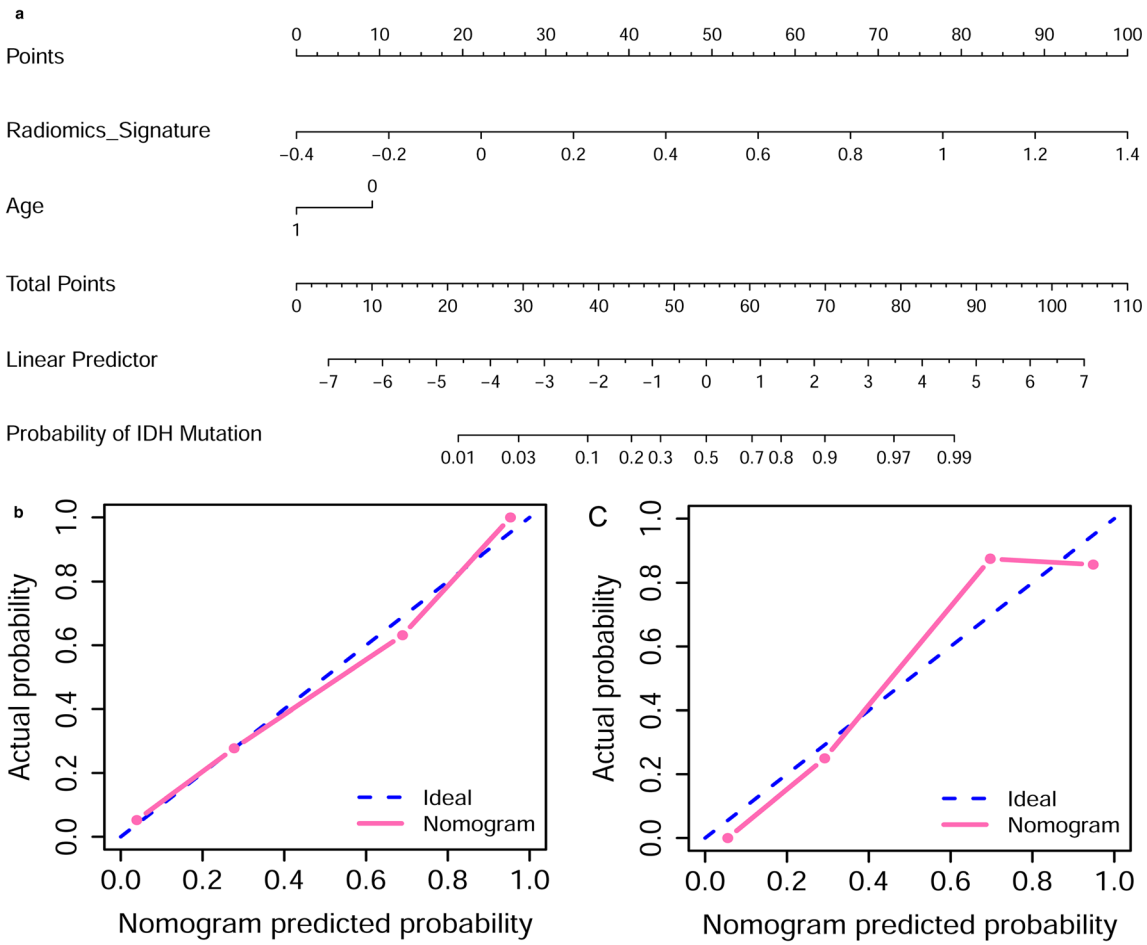

Fig. 5 **a** The radiomics nomogram. Calibration curves in the training cohort (**b**) and validation cohort (**c**). The diagonal blue line represents an ideal evaluation, while the pink lines represent the performance of the nomogram. Closer fit to the diagonal blue line indicates a better evaluation

features from CE-T1WI had better predictive performance than those from the ADC map. The one reason might be that the image resolution of the ADC map was lower than the CE-T1WI images, which influenced the stability and robustness of the radiomics features. The other one might be that the DWI sequence had inconsistent performance and was not a stable indicator for glioma grading or molecular subtype according to the literatures [38–40].

Recent radiomics studies of IDH prediction focused on Grade II gliomas [17–19] or high-grade gliomas with highest accuracy of 86% [20, 21], which used hundreds of radiomics features mainly from tumor area and needed tumor grading as a prerequisite, but the grade information would not be confirmed without pathological tissue after invasive surgery or biopsy. As we all know that one main characteristic of radiomics is noninvasive, while with tumor grading as a prerequisite would limit its clinical application. Some studies have reported that IDH genotype may be independent of astrocytoma grade [13, 41]. Our results confirmed the hypothesis that the radiomics approach from multiparametric and multiregional MR images could predict the IDH genotype when expanding the cohort to Grades II–IV astrocytomas, and with superior AUC of 0.913. Furthermore, when restricting our cohort to low-grade or high-grade astrocytomas for predicting IDH genotype, the AUC reached 0.874 and 0.928 respectively. Our radiomics model without tumor grading as a prerequisite greatly compensated the previous studies, which would accelerate its clinical application.

The combined model incorporating the radiomics signature and age performed better than the clinico-radiological model, which demonstrated the incremental value of the radiomics signature in predicting IDH genotype for astrocytomas. It was important to note that the age demonstrated sufficient predictive strength and could be easily obtained preoperatively [42], which made the inclusion of this variable a common strategy for the development of combined model. Furthermore, we used a nomogram to visualize the preoperative prediction for the IDH genotype which has not been reported. The nomogram of the combined model might be an effective and easy-to-use tool to estimate the IDH genotype before surgery, especially for patients who were not able to undergo biopsy or surgery.

Table 4 The characteristics of high-risk and low-risk astrocytomas in the survival analysis

Characteristic	High-risk ($N = 37$)	Low-risk ($N = 24$)	p value
Age (Years)	58.76 ± 11.69	44.29 ± 8.13	< 0.001
Gender			0.322
Male	23 (62.16%)	11 (45.83%)	
Female	14 (37.84%)	13 (54.17%)	
Grade			0.004
II	9 (24.32%)	16 (66.67%)	
III	19 (51.35%)	6 (25.00%)	
IV	9 (24.32%)	2 (8.33%)	
Radiotherapy and/or chemotherapy*			0.494
Yes	17 (45.95%)	14 (58.33%)	
No	20 (54.05%)	10 (41.67%)	
IDH genotype			< 0.001
IDH-M	6 (16.22%)	20 (83.33%)	
IDH-W	31 (83.78%)	4 (16.67%)	
OS (median [range], days)	460 (95–1991)	1220 (183–2022)	< 0.001

IDH-M IDH mutation astrocytomas, *IDH-W* IDH wild type astrocytomas, *OS* overall survival

The high-risk and low-risk groups were defined based on the score of the combined model developed by incorporating age, edema degree, and radiomics signature (predictive model for IDH genotype). For high-risk group, the score of combined model was less than cutoff; for low-risk group, that was larger than cutoff

*all the patients underwent surgery, and 31 of 61 patients had further radiotherapy and/or chemotherapy after surgery

Furthermore, we evaluated the prognostic value of combined model, which is a very good supplement to current radiomics studies of IDH genotype for the real clinical relevance. In our study, IDH-M astrocytomas gained more benefits from conventional treatments and were associated with longer OS compared with IDH-M ones independent of pathological grade, which was consistent with previous studies that IDH genotype was an important prognostic hallmark for astrocytomas [1–4]. Our combined model also stratified astrocytomas into high- and low- risk groups, and its prognostic value showed no difference with IDH genotype. This further confirmed that the combined model was sufficiently accurate to predict IDH genotype and demonstrated considerable prognostic value, which might contribute to the pretreatment decision-making including surgery and adjuvant treatment plans, especially for the upcoming targeted therapy.

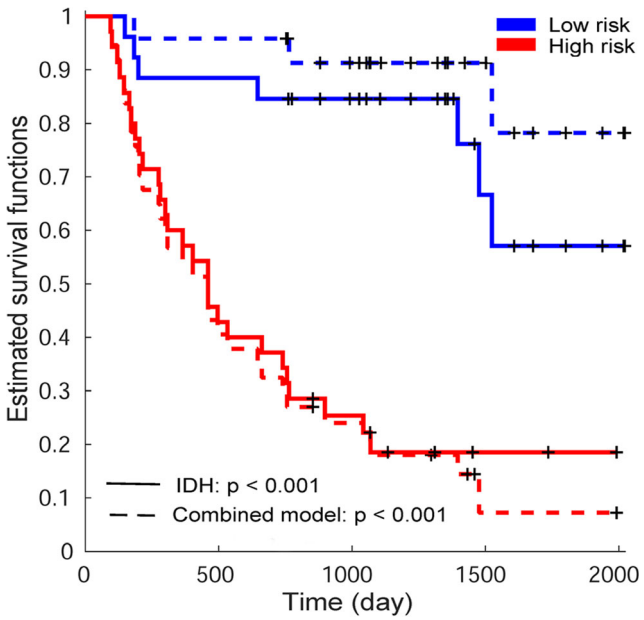

Fig. 6 Kaplan–Meier survival analysis of the combined model. The combined model (dotted line) successfully stratified astrocytomas into high-risk (red line) and low-risk (blue line) groups with a significant prognostic difference, which was similar with the performance of IDH genotype (solid line)

Despite the promising results, our study also had several limitations. First, we used retrospective data from a single-institution to train and validate the predictive model. Multicenter data should be collected to test the stable performance of the model. Second, we only focused on IDH genotype of tumor. With increased cases, the relationship between imaging characteristics and meta-gene abnormal expressions such as MGMT and TP53 should be investigated. Third, our study was based on a retrospective analysis; we selected the highest grading part of the tumor to analysis IDH genotype. The intra-lesion heterogeneity of IDH was not studied. Finally, we focused on the conventional sequences; other advanced sequences such as dynamic susceptibility-weighted contrast-enhanced (DSC) perfusion-weighted imaging or diffusion tension imaging were not included.

In conclusion, the radiomics nomogram could predict the IDH genotype for Grades II–IV astrocytomas with high accuracy, and could perform risk stratification for astrocytomas according to OS. Thus, the radiomics nomogram might be a useful supporting tool in preoperatively predicting the IDH genotype for astrocytomas, which could aid treatment decision-making and prognosis-evaluating.

Funding This study has received funding by the National Natural Science Foundation (81471652 and 81771824 to Hui Zhang; 81227901, 81527805, 61231004, and 81671851 to Jie Tian; 81701681 to Yan Tan; 81771924, 81501616 to Di Dong; 11705112 to Guo-qiang Yang); National Key R&D Program of China (2017YFA0205200 and 2017YFC1309100 to Jie Tian, 2017YFC1308700 to Di Dong); the Precision Medicine Key Innovation Team Project (YT1601 to Hui Zhang); the Social Development Projects of Key R&D Program in Shanxi Province (201703D321016 to Hui Zhang); and the Natural Science Foundation of Shanxi Province (201601D021162 to Yan Tan).

Compliance with ethical standards

Guarantor The scientific guarantor of this publication is Hui Zhang.

Conflict of interest The authors of this manuscript declare no relationships with any companies, whose products or services may be related to the subject matter of the article.

Statistics and biometry One of the authors has significant statistical expertise.

Informed consent Written informed consent was not required for this study because this is a retrospective study and patient data are anonymized.

Ethical approval Institutional Review Board approval was obtained.

Methodology
- retrospective
- diagnostic or prognostic study
- performed at one institution

References

1. Ichimura K, Narita Y, Hawkins CE (2015) Diffusely infiltrating astrocytomas: pathology, molecular mechanisms and markers. Acta Neuropathol 129(6):789–808
2. Louis DN, Perry A, Reifenberger G et al (2016) The 2016 world health organization classification of tumours of the central nervous system: a summary. Acta Neuropathol 131(6):803–820
3. Rogers TW, Tsui A, Gonzales M (2018) Re-classification of gliomas by the 2016 revision of the who classification of CNS tumours. Pathology 50(Sup1):S123
4. Brat DJ, Verhaak RG, Aldape KD et al (2015) Comprehensive, integrative genomic analysis of diffuse lower-grade gliomas. N Engl J Med 372(26):2481–2498
5. Beiko J, Suki D, Hess KR et al (2014) IDH1 mutant malignant astrocytomas are more amenable to surgical resection and have a survival benefit associated with maximal surgical resection. Neuro Oncol 16(1):81–91
6. Kizilbash SH, Giannini C, Voss JS et al (2014) The impact of concurrent temozolomide with adjuvant radiation and IDH mutation status among patients with anaplastic astrocytoma. J Neurooncol 120(1):85–93
7. Tran AN, Lai A, Li S et al (2016) Increased sensitivity to radiochemotherapy in IDH1 mutant glioblastoma as demonstrated by serial quantitative MR volumetry. Neuro Oncol 16(3):414–420
8. Rohle D, Popovici-Muller J, Palaskas N et al (2013) An inhibitor of mutant IDH1 delays growth and promotes differentiation of glioma cells. Science 340(6132):626–630
9. Waitkus MS, Dilpas BH, Yan H (2018) Biological role and therapeutic potential of IDH mutation in cancer. Cancer Cell. https://doi.org/10.1061/j.ccell.2-18.04.011
10. Andronesi OC, Arrillaga-Romany IC, Ina Ly K et al (2018) Pharmacodynamics of mutant-IDH1 inhibitors in glioma patients probed by in vivo 3D MRS imaging of 2-hydroxyglutarate. Nat Commun 9:1474. https://doi.org/10.1038/s41467-018-03905-6
11. Sullivan DC, Obuchowski NA, Kessler LG et al (2015) Metrology standards for quantitative imaging biomarkers. Radiology 277(3):813–825
12. Liu Z, Zhang Y, Yan H et al (2012) Altered topological patterns of brain networks in mild cognitive impairment and Alzheimer's disease: a resting-state fMRI study. Psychiat Res-Neuroim 202(2):118–125
13. Qi S, Yu L, Li H et al (2014) Isocitrate dehydrogenase mutation is associated with tumour location and magnetic resonance imaging characteristics in astrocytic neoplasms. Oncol Lett 7(6):1895–1902
14. Metellus P, Coulibaly B, Colin C et al (2010) Absence of IDH mutation identifies a novel radiologic and molecular subtype of WHO grade II gliomas with dismal prognosis. Acta Neuropathol 120(6):719–729
15. Gillies RJ, Kinahan PE, Hricak H (2015) Radiomics: images are more than pictures, they are data. Radiology 278(2):563–577
16. Lambin P, Leijenaar RTH, Deist TM et al (2017) Radiomics: the bridge between medical imaging and personalized medicine. Nat Rev Clin Oncol 14:947–762
17. Yu J, Shi Z, Lian Y et al (2017) Noninvasive IDH1 mutation estimation based on a quantitative radiomics approach for grade II glioma. Eur Radiol 27(8):3509–3522
18. Li Z, Wang Y, Yu J, Guo Y, Cao W (2017) Deep learning based radiomics (DLR) and its usage in noninvasive IDH1 prediction for low grade glioma. Sci Rep 7(1):5467
19. Zhang X, Tian Q, Wang L et al (2018) Radiomics strategy for molecular subtype stratification of lower-grade glioma: detecting IDH and TP53 mutations based on multimodal MRI. J Magn Reson Imaging. https://doi.org/10.1002/jmri.25960
20. Zhang B, Chang K, Ramkissoon S et al (2017) Multimodel MRI features predict isocitrate dehydrogenase genotype in high-grade gliomas. Neuro Oncol 19(1):109–117
21. Hsieh KL, Chen CY, Lo CM (2017) Radiomic model for predicting mutations in the isocitrate dehydrogenase gene in glioblastomas. Oncotarget 8(28):45888–45897
22. Baldock AL, Yagle K, Born DE et al (2014) Invasion and proliferation kinetics in enhancing gliomas predict IDH1 mutation status. Neuro Oncol 16(6):779–786
23. Chen J, Tian J (2009) Real-time multi-modal rigid registration based on a novel symmetric-SIFT descriptor. Prog Nat Sci 19(5):643–651
24. Gebejes A, Huertas R (2013) Texture characterization based on grey-level co-occurrence matrix. International Conference on Information and Communication Technologies 1:375–378
25. Galloway MM (1975) Texture analysis using gray level run lengths. Computer Graphics and Image Processing 4:172–179
26. Chu A, Sehgal CM, Greenleaf JF (1990) Use of gray value distribution of run lengths for texture analysis. Pattern Recognit Lett 11:415–419

27. Dasarathy BV, Holder EB (1991) Image characterizations based on joint gray level—run length distributions. Pattern Recognit Lett 12: 497–502
28. Thibault G, Fertil B, Navarro C et al (2013) Shape and texture indexes application to cell nuclei classification. Intern J Pattern Recognit Artif Intell 27:1357002
29. Thibault G, Fertil B, Navarro C et al (2009) Texture indexes and gray level size zone matrix: application to cell nuclei classification. Pattern Recognition Inf Process 140–145
30. Amadasun M, King R (1989) Textural features corresponding to textural properties. IEEE Trans Syst Man Cybern 19:1264–1274
31. Zhang B, Tian J, Dong D et al (2017) Radiomics features of multiparametric MRI as novel prognostic factors in advanced nasopharyngeal carcinoma. Clin Cancer Res 23(15):4259–4269
32. Chalkidou A, O'Doherty MJ, Marsden PK et al (2015) False discovery rates in PET and CT studies with texture features: a systematic review. PLoS One 10(5):e0124165
33. Rathore S, Akbari H, Doshi J et al (2018) Radiomic signature of infiltration in peritumoural edema predicts subsequent recurrence in glioblastoma: implications for personalized radiotherapy planning. J Med Imaging (Bellingham) 5(2):021219. https://doi.org/10.1117/1.JMI.5.2.021219
34. Prasanna P, Patel J, Partov S, Anant Madabhushi A, Tiwari R (2017) Radiomic features from the peritumoural brain parenchyma on treatment-naïve multi-parametric MR imaging predict long versus short-term survival in glioblastoma multiforme: preliminary findings. Eur Radiol 27:4188–4197
35. Parsons DW, Jones S, Zhang X et al (2008) An integrated genomic analysis of human glioblastoma multiforme. Science 321(5897): 1807–1812
36. Dang L, Yen K, Attar EC (2016) IDH mutations in cancer and progress toward development of targeted therapeutics. Ann Oncol 27(4):599–608
37. Colen R, Ashour O, Zinn PO (2013) Imaging genomic IDH-1 biomarker signature. Neuro Oncol 15(Suppl 3):iii191–iii205
38. Santelli L, Ramondo G, Della Puppa A et al (2010) Diffusion-weighted imaging does not predict histological grading in meningiomas. Acta Neurochir (Wien) 152(8):1315–1319
39. Lam WW, Poon WS, Metreweli C (2002) Diffusion MR imaging in glioma: does it have any role in the pre-operation determination of grading of glioma. Clin Radiol 57(3):219–225
40. Xing Z, Yang X, She D, Lin Y, Zhang Y, Cao D (2017) Noninvasive assessment of IDH mutational status in World Health Organization Grade II and III Astrocytomas using DWI and DSC-PWI combined with conventional MR imaging. AJNR Am J Neuroradiol 38(6): 1138–1144
41. Turcan S, Rohle D, Goenka A et al (2012) IDH mutation is sufficient to establish the glioma hypermethylator phenotype. Nature 483(7390):479–483
42. Reuss DE, Mamatjan Y, Schrimpf D et al (2015) IDH mutant diffuse and anaplastic astrocytomas have similar age at presentation and little difference in survival: a grading problem for WHO. Acta Neuropathol 129(6):867–873